BRIEF COMMUNICATION

Endogenous ZAP affects Zika virus RNA interactome

Ahmad Jawad Sabir[1,a], Nguyen Phuong Khanh Le[2,a], Prince Pal Singh[2,3,a], Uladzimir Karniychuk[2,*]

[1]Department of Microbiology and Immunology, University of Illinois, College of Medicine, Chicago, IL, USA

[2]Department of Veterinary Biosciences, College of Veterinary Medicine, The Ohio State University, Columbus, OH, USA

[3]School of Public Health, University of Saskatchewan, Saskatoon, Canada

[a]**:** These authors contributed equally

*** Correspondence:** Uladzimir Karniychuk
Department of Veterinary Biosciences, College of Veterinary Medicine, The Ohio State
University, Columbus, OH, USA
karniychuk.1@osu.edu

Abstract

One of the most recent advances in analysis of viral RNA–cellular protein interactions is the Comprehensive Identification of RNA-binding Proteins by Mass Spectrometry (ChIRP-MS). Here, we used ChIRP-MS in mock-infected and Zika-infected wild-type cells and cells knockout for the zinc finger CCCH-type antiviral protein 1 (ZAP). We characterized "ZAP-independent" and "ZAP-dependent" cellular protein interactomes associated with flavivirus RNA and found that ZAP affects cellular proteins associated with Zika virus RNA. Accordingly, we showed that in the same experimental system ZAP affects infection phenotypes of Zika virus, and other flaviviruses—Japanese encephalitis virus and West Nile virus. The ZAP-dependent interactome identified with ChIRP-MS provides potential ZAP co-factors for antiviral activity against Zika virus and possibly other viruses. Identifying the full spectrum of ZAP co-factors and mechanisms of how they act will be critical to understand the ZAP antiviral system and may contribute to the development of antivirals.

Keywords: Flavivirus, Zika virus, Japanese encephalitis virus, West Nile virus, Zinc finger antiviral protein, ZAP, RNA, interactome

INTRODUCTION

Emerging flaviviruses constantly threaten public health. The National Institute of Allergy and Infectious Diseases classifies flaviviruses— Zika virus, Japanese encephalitis virus (JEV), yellow fever virus (YFV), and West Nile virus (WNV) as a "Category B Priority," the 2nd highest priority of emerging pathogens and biodefense threats. Zika virus caused the human epidemic in 2015 and persists in at least 89 countries. Japanese encephalitis virus causes encephalitis in humans in the Asia-Pacific region [1], with 68,000 annual cases and 15,000 deaths [2]. There is a concern that JEV can be introduced into North America given the large population of amplifying hosts—pigs and wild boars, and susceptible *Culex* mosquitoes [3-5]. Japanese encephalitis virus keeps expanding—the 2022 JEV outbreak in Australia with infections in swine herds, zoonotic transmission, and human deaths was caused by genotype IV which was not associated with outbreaks before [6]. West Nile virus is the most common arthropod-borne virus in the USA. In 2022, there were 1,126 cases, including 93 deaths. In 2023, 2,406 human cases were reported in the US, with 1,599 neuroinvasive diseases. The rising number of human cases caused by mosquito-borne flaviviruses shows the lack or inefficiency of environmental controls. There are no approved human vaccines for some flaviviruses (i.e., Zika, WNV). Also, there are no licensed antivirals against flaviviruses because of a knowledge gap in cellular pathways controlling infections, including the knowledge gap in interactions of viral RNA with cellular proteins.

High-throughput methods enable global analysis of viral RNA–cellular protein interactions. One of the most recent advances in analysis of viral RNA–cellular protein interactions is the Comprehensive Identification of RNA-binding Proteins by Mass Spectrometry (ChIRP-MS) [7], where interactions between cellular proteins and genomic RNA of several viruses were profiled that substantially advanced the fundamental knowledge of RNA viruses and informed novel antivirals [8-11]. To our knowledge, all these ChIRP-MS studies were done in wild-type cell lines. And comparative ChIRP-MS studies on viral RNA–cellular protein interactions in wild-type and knock-out (KO) cell lines are not reported.

The zinc finger CCCH-type antiviral protein 1, also known as ZAP, ZC3HAV1, or PARP13, is one of the major cellular proteins with broad antiviral activity. The protein was first characterized to inhibit murine leukemia virus [12] and later alphaviruses, filoviruses, influenza virus, porcine reproductive and respiratory syndrome virus, hepatitis B virus, human cytomegalovirus, human T cell leukaemia virus type 1, and HIV-1 [13-23]. ZAP binds viral RNA and evokes antiviral activity by mediating viral RNA degradation and translational inhibition [24].

Here, we used the ChIRP-MS in mock-infected and Zika-infected wild-type and ZAP-KO cells and characterized “ZAP-independent” and “ZAP-dependent” cellular protein interactomes associated with flavivirus RNA. We found that ZAP affects cellular proteins associated with Zika virus RNA. Accordingly, we showed that in the same experimental system ZAP affects infection phenotypes of Zika virus, and other flaviviruses—JEV and WNV.

RESULTS

ChIRP-MS uncovers ZAP-dependent Zika virus RNA interactome

To define the ZAP-depended host protein interactome associated with Zika genomic RNA, we used the RNA-directed proteomic discovery method ChIRP-MS [7-11] in VERO wild-type (VERO-ZAP-WT) and knock-out (VERO-ZAP-KO) cell lines. We crosslinked mock-infected and virus-infected cell lines with formaldehyde to preserve viral RNA–protein complexes and applied biotinylated oligonucleotides (**Table S1A**) tiling the entire Zika virus RNA to enrich viral RNA–host protein complexes (**Fig 1A**).

Before comparing viral RNA–host protein interactions, we tested different Zika MOIs for inoculation of ZAP-WT and ZAP-KO cells to ensure similar viral RNA loads at the time of formaldehyde fixation and accurate comparative ChIRP-MS. The multiplicity of infection 10 for VERO-ZAP-WT cells and MOI 2 for VERO-ZAP-KO cells evoke similar Zika virus loads. To exclude the effects of differential uptake of the stimulus during MOI 10 inoculation of VERO-ZAP-WT cells, during VERO-ZAP-KO MOI 2 inoculation we added heat-inactivated Zika virus equivalent of MOI 8. After extensive washing and 72 h incubation, the same Zika antigen loads in VERO-ZAP-WT and VERO-ZAP-KO cells were confirmed with viral E protein staining (**Fig 1B**). The same Zika RNA loads in VERO-ZAP-WT and VERO-ZAP-KO cells were also confirmed using Zika-specific RT-qPCR and next-generation-sequencing (NGS) in sonicated cellular lysates (input) and immunoprecipitated viral RNA-protein complexes (enriched) (**Figs 1C, D**). High RT-qPCR Zika loads and nearly entire Zika genomic coverage with high NGS depth (**Figs 1C, D**) confirms that the ChIRP method efficiently recovered the same high loads of viral RNA in both VERO-ZAP-WT and VERO-ZAP-KO cells. Also, as expected, viral RNA loads were consistently higher in enriched than in input samples in RT-qPCR and NGS assays (**Figs 1C, D**). Altogether, we confirmed normalized viral loads, the similar binding capacity and enrichment of viral RNA during ChIRP in VERO-ZAP-WT and VERO-ZAP-KO cells, and the validity of the quantitative comparison of proteins associated with viral RNA between wild-type and ZAP-KO cells.

We applied three analytical strategies and MiST to analyze ChIRP-MS data. For the first analytical strategy, using the raw ChIRP-MS data with a total of 2,269 proteins (**Table S1B**), we identified proteins specifically associated with Zika virus RNA in VERO-ZAP-WT cells. For specificity, we selected the Singleton Filtering MiST option to exclude proteins with spectral counts in only one biological replicate (out of three replicates) and quantify proteins with a MiST score of 0.75 or above [11,25,26]. Also, to increase the specificity, we excluded all proteins that had at least a single spectral count in at least one of three biological replicates in mock-infected wild-type or ZAP-KO cells. We defined the resultant list of enriched proteins as the "extended" Zika virus RNA interactome in VERO-ZAP-WT cells. This extended interactome contains 383 proteins (**Table S1C**). We named this interactome "extended" because additional control criteria were applied to narrow down and enrich the "ZAP-dependent" Zika virus RNA interactome (see below). ChIRP-MS is a rather new technique in molecular biology; the first time it was described for systemic identification of cellular proteins interacting with cellular mRNA in 2015 [7]. From 2019, several virology groups applied ChIRP-MS to characterize interactions between cellular proteins and genomic RNA of severe acute respiratory syndrome coronavirus 2, Ebola virus, dengue virus, and Zika virus in wild-type ZAP-positive cells [8-11]. Thus, we compared our extended Zika virus RNA interactome in VERO-ZAP-WT cells with the Zika interactome in Huh cells from a previous publication [10]. A similar number of proteins was reported here—383, and previously—395. The comparison also showed a good reproducibility of 25.4 % between two protein sets (**Table S1D**). We consider 25.4% a good reproducibility because studies were done in cells of different species—nonhuman primates (VERO) and humans (Huh), with different MOIs and sampling time points. The specificity of our ChIRP-MS is also confirmed by physical associations between Zika virus RNA and viral prM, C, E, NS1, NS2A, NS2B, NS3, and NS5 proteins in only infected cells, while all mock-infected replicates were negative (**Table S1E**). The enrichment of viral proteins provides evidence that ChIRP-MS covers interactions across the entire length of viral RNA [8]. Analysis of the MiST abundance score and absolute spectral counts showed that the viral NS3 and NS5 proteins were most strongly recovered (**Table S1E**; NS3 MiST abundance score 0.167, NS5 MiST abundance score 0.304; NS3 mean spectral counts 39, NS5 mean spectral counts 102), which is consistent with previous ChIRP-MS Zika virus study where NS3 and NS5 were also most abundant [10]; and with direct binding function of flavivirus NS3—RNA helicase, and NS5— RNA-dependent RNA polymerase. Analyzes of top interacting cellular proteins with the highest spectral counts and GO enrichment analysis also suggested the specificity of ChIRP-MS. All top 15 interacting proteins (except NCOA5) with the highest spectral counts (**Fig 2A**) are known factors of RNA biology, including RNA binding, RNA splicing, and RNA helicase activities (**Table S1C**). Gene Ontology enrichment analysis also showed that all seven enriched pathways with at least two-fold enrichment represent nucleic acid/RNA binding and RNA biology processes (**Fig 2D**).

For the second analytical strategy, we identified proteins specifically interacting with Zika virus RNA in VERO-ZAP-KO cells. For specificity, we applied the same strategy as above: We selected the Singleton Filtering MiST option to exclude proteins with spectral counts in only one biological replicate and quantify proteins with the MiST score of 0.75 or above [11,25,26]. We also excluded all proteins with a single spectral count in at least one of three biological replicates in mock-infected wild-type or ZAP-KO cells. We defined the resultant list of enriched proteins as a "ZAP-independent" Zika virus RNA interactome. We defined this interactome as ZAP-independent because associated cellular proteins were discovered in VERO-ZAP-KO cells showing the ZAP-independent nature of interactions. The ZAP-independent interactome contains 116 proteins

(**Table S1F**). As expected, most, 13 out of 15 top cellular interacting proteins with the highest spectral counts are known factors in RNA biology (**Fig 2B**; **Table S1F**). Zika virus proteins were identified in only infected VERO-ZAP-KO cells (**Table S1G**).

Finally, to discover the "ZAP-dependent" Zika RNA interactome in VERO-ZAP-WT cells, in addition to the above specificity exclusion criteria in MiST settings and mock-infected cells, we excluded proteins that had at least one spectral count in at least one of the three biological replicates in VERO-ZAP-KO cells infected with Zika virus. The ZAP-dependent interactome contains 209 proteins (**Table S1H**). The ZAP-dependent Zika RNA interactome has more proteins than ZAP-independent—209 versus 116 proteins. As expected, most, 12 out of 15 top interacting proteins with the highest spectral counts in the ZAP-dependent interactome are known factors in RNA biology (**Fig 2C**; **Table S1H**). Comparative GO enrichment analysis between ZAP-independent and ZAP-dependent interactomes showed only one enriched pathway related to RNA biology in ZAP-KO cells and six enriched RNA biology pathways in ZAP-WT cells, including "helicase activity" with the highest fold enrichment (**Figs 2E, F**). Accordingly, among the top 15 proteins in the ZAP-dependent interactome four proteins were RNA helicases (**Table S1H**). In total, 11 RNA helicases were enriched in the ZAP-dependent interactome—DDX42, DDX56, DDX27, DDX50, DDX52, DDX23, DDX54, DDX18, DHX57, DDX47, and one uncharacterized RNA helicase (**Tables S1H, I**). In the ZAP-independent interactome, no RNA helicases were enriched.

Endogenous ZAP affects flavivirus infection phenotypes

The different Zika virus RNA interactomes in ZAP-WT and ZAP-KO cells (**Fig 2**; **Table S1**) motivated as to test whether endogenous ZAP inhibits Zika virus infection in VERO cells. Zika virus showed reduced infection loads in VERO-ZAP-WT compared to VERO-ZAP-KO cells (**Fig 3**): Virus envelop (E) protein-positive cells (**Figs 3B**, **D**, and **G**), extracellular viral RNA (**Figs 3C** and **F**), and NS5 protein (**Fig 3E**) were reduced. Next, we compared alongside infection phenotypes of three flaviviruses in VERO-ZAP-WT and VERO-ZAP-KO cells— JEV previously shown to be sensitive to endogenous and ectopically overexpressed ZAP; Zika virus previously designated as ZAP-resistant; and WNV with unknown sensitivity to ZAP in VERO cells. For all flaviviruses, we observed a significant ($p < 0.0001$) reduction in E protein expression in VERO-ZAP-WT compared to VERO-ZAP-KO cells (**Figs 4A**, **B**, **E**, **F**, **I**, **J**, and **S1 Fig**). All three flaviviruses also showed a considerable reduction of NS5 protein expression in VERO-ZAP-WT compared to VERO-ZAP-KO cells (**Figs 4D**, **H**, **L**). In contrast to E and NS5 protein expression reduction, WNV had comparable intracellular viral RNA loads (p = 0.1875) in VERO-ZAP-WT and VERO-ZAP-KO cells (**Fig 4K**). In agreement with the reduction of E and NS5 protein expression, Zika virus and JEV had significantly ($p = 0.0012$ and 0.0007) higher intracellular RNA loads in VERO-ZAP-KO than in VERO-ZAP-WT lines (**Figs 4C, G**).

DISCUSSION

There are two key findings in this study. First, using ChIRP-MS in ZAP-WT and ZAP-KO cells, we delineated ZAP-independent and ZAP-dependent cellular protein interactomes associated with Zika virus RNA. Second, we showed that endogenous ZAP affects Zika virus and WNV infection phenotypes.

All previous ChIRP-MS studies of a viral RNA-cellular protein interactome were done in wild-type cell lines [8-11], and comparative ChIRP-MS studies in wild-type and KO cells were not reported. Here, we showed that such experimental approach is feasible by normalizing MOIs and viral loads in ZAP-WT and ZAP-KO cells, and identified ZAP-independent and ZAP-dependent Zika virus RNA interactomes. To our knowledge, this is also the first ZAP-dependent interactome study in the context of viral infection. Interestingly, the ZAP-dependent interactome showed a considerably higher number of cellular proteins associated with viral RNA than the ZAP-independent interactome (209 versus 116 proteins). The difference in 93 proteins between interactomes in ZAP-WT and ZAP-KO cells is rational because in the previous study a tandem mass spectrometry showed that 114 cellular proteins interact with the overexpressed immunoprecipitated ZAP large isoform in uninfected cells [27]. Other large-scale interactome studies in non-infected cells have identified more than 250 potential cellular proteins that may potentially interact with ZAP [27-31]. In addition to quantitative changes, ZAP also affected Zika RNA interactome qualitatively. Interestingly, 11 RNA helicases were enriched in the ZAP-dependent interactome—DDX42, DDX56, DDX27, DDX50, DDX52, DDX23, DDX54, DDX18, DHX57, DDX47, and one uncharacterized RNA helicase. In contrast, in the ZAP-independent interactome, no RNA helicases were enriched. The limitation is that our experimental design does not allow to identify the specific nature of interactions between Zika virus RNA and cellular proteins. We do not know yet which cellular proteins interact with only ZAP bound to viral RNA, which interact with ZAP and viral RNA, and which proteins have strict viral RNA dependency during interactions with ZAP. ZAP binds to single-stranded viral RNA and potentially to single overhangs in double RNA [32,33]; RNA helicases can bind to double-stranded RNA, single overhangs in double RNA, and single-stranded RNA; these make interactions between ZAP, viral RNA, and RNA helicases spatially possible. It is known that DDX RNA helicases not only facilitate viral RNA degradation but also act as viral RNA sensing proteins contributing to cellular innate immune signaling, type I IFN production, and antiviral response [34-39]. Also, viruses can abduct cellular RNA helicases to support their lifecycle and promote infectivity [40,41]. Cellular RNA helicases often interact with microbial genomes and evoke their properties in the complex with different adaptor proteins [34-36,38,42-44]. Thus, ZAP may play a dual role in mediating RNA helicase-dependent antiviral and proviral effects. Some RNA helicases are co-factors required for ZAP activity (see below). But before our ChIRP-MS study, the co-factor/adaptor role of ZAP in interactions between viral RNA and cellular RNA helicases was not considered.

Being a potential co-factor for RNA helicases, ZAP itself requires them as co-factors. ZAP's N-terminus interacts with the N- and C-terminal domains of DDX17 that promotes ZAP-mediated degradation of murine leukemia reporter virus [45]. However, our ChIRP-MS Zika data do not contain p72 DEAD-box RNA helicase (DDX17) (**Table S1B**). DHX30 interacts with ZAP, and the knockdown of DHX30 reduces ZAP's antiviral activity against murine leukemia reporter virus [46]. Accordingly, we identified DHX30 in ChIRP-MS data (**Table S1B**); however, it was excluded from further interactome-specific analysis with our rigorous specificity cutoff.

In addition to RNA helicases, ZAP requires other co-factors. It lacks intrinsic RNase activity but recruits the 5' and 3' RNA degradation machinery [47,48]. The E3 ubiquitin ligase TRIM25 is important for ZAP activity against alphaviruses by increasing inhibition of viral translation [49,50]. ZAP also interacts with the cytoplasmic protein KHNYN to inhibit CpG-enriched HIV-1 [51]. Riplet, a protein known to play a central role in activating the retinoic acid-inducible gene I (RIG-I), has been recently identified as a ZAP co-factor that augments the restriction of HIV-1 [52]. However, the full complexity of cellular proteins essential for ZAP antiviral activity is unknown. Again, large-scale interactome studies in non-infected cells have identified more than 250 proteins that may interact with ZAP [27-31]. Notably, there were no large-scale ZAP interactome studies in the context of viral infection [28]. Our ZAP-dependent ChIRP-MS interactome (**Table S1H**) provides a highly specific list of potential ZAP co-factors, including eleven RNA helicases for future mechanistic and functional studies.

The previous ZAP overexpression study showed JEV sensitivity to ectopic ZAP, and insensitivity of Zika virus [48]. The sensitivity of Zika virus was previously tested to ectopically overexpressed ZAP against the background of endogenous ZAP [48]. Overexpression screening is a powerful approach, but overexpressing individual genes may also miss antiviral effectors that work in multiprotein complexes [53]. Indeed, it is known that ZAP can augment other antiviral systems [14]. Different cell lines were also used: Previously, the authors used A549 cells isolated from human cancer lung tissue [48], and we used VERO cells from a healthy monkey. Indeed, antiviral signaling for many cellular proteins can be highly cell-specific [54]. Another potential factor is that the human cell line was used previously, and here, we used the African green monkey (a possible natural reservoir host of Zika virus [55]) cell line. Species-specific ZAP effects are known [56,57]; however, there are no comparative studies on ZAP antiviral activity between primates. Finally, previously the authors used 10 h and 24 h sampling times; here, we sampled infected ZAP-WT and ZAP-KO cells at 24 h and 72 h after Zika infection (**Figs 3, 4**), and later effects suggest indirect ZAP-mediated antiviral activity.

Together, the ZAP-dependent interactome identified with ChIRP-MS provides potential ZAP co-factors for antiviral activity against Zika virus and possibly other viruses. Identifying the full spectrum of ZAP co-factors and mechanisms of how they act will be critical to understand the ZAP antiviral system and may contribute to the development of antivirals.

MATERIALS AND METHODS

Details of ChIRP-MS, cells, viruses, comparative infection studies, RT-qPCR, western blot, and statistics are in supplementary materials and methods.

DISCLOSURE STATEMENT

The authors declare that the research was conducted in the absence of any commercial or financial relationships that could be construed as a potential conflict of interest.

AUTHOR CONTRIBUTIONS

Conceptualization: UK. Investigation: NPKL, AJS, PPS, UK. Data analysis: NPKL, AJS, PPS, UK. Funding: UK. Resources: UK. Writing—original draft preparation: NPKL, AJS, PPS, UK. Writing—review and editing: UK.

FUNDING

PPS received a Scholarship from the School of Public Health, University of Saskatchewan. This work was partially supported by a grant to UK from the Canadian Institutes of Health Research (CIHR; Project Grant #424307). The funders had no role in study design, data collection and analysis, decision to publish, or manuscript preparation.

DATA AVAILABILITY

Data available within the article or its supplementary materials.

REFERENCES

1. Amicizia D, Zangrillo F, Lai PL, et al. Overview of Japanese encephalitis disease and its prevention. Focus on IC51 vaccine (IXIARO®). Journal of Preventive Medicine and Hygiene. 2018;59:E99-E107.
2. Tarantola A, Goutard F, Newton P, et al. Estimating the burden of Japanese encephalitis virus and other encephalitides in countries of the mekong region. PLoS neglected tropical diseases. 2014;8:e2533.
3. Oliveira ARS, Piaggio J, Cohnstaedt LW, et al. Introduction of the Japanese encephalitis virus (JEV) in the United States – A qualitative risk assessment. Transboundary and Emerging Diseases. 2019;66:1558-1574.
4. Huang YJS, Harbin JN, Hettenbach SM, et al. Susceptibility of a North American Culex quinquefasciatus to Japanese Encephalitis Virus. Vector borne and zoonotic diseases (Larchmont, NY). 2015;15:709-711.
5. Faizah AN, Kobayashi D, Matsumura R, et al. Blood meal source identification and RNA virome determination in Japanese encephalitis virus vectors collected in Ishikawa Prefecture, Japan, show distinct avian/mammalian host preference. J Med Entomol. 2023 Apr 7.
6. Howard-Jones AR, Pham D, Jeoffreys N, et al. Emerging Genotype IV Japanese Encephalitis Virus Outbreak in New South Wales, Australia. Viruses. 2022 Aug 24;14(9).
7. Chu C, Zhang QC, da Rocha ST, et al. Systematic discovery of Xist RNA binding proteins. Cell. 2015 Apr 9;161(2):404-16.
8. Flynn RA, Belk JA, Qi Y, et al. Discovery and functional interrogation of SARS-CoV-2 RNA-host protein interactions. Cell. 2021 Apr 29;184(9):2394-2411 e16.
9. Labeau A, Fery-Simonian L, Lefevre-Utile A, et al. Characterization and functional interrogation of the SARS-CoV-2 RNA interactome. Cell Rep. 2022 Apr 26;39(4):110744.
10. Ooi YS, Majzoub K, Flynn RA, et al. An RNA-centric dissection of host complexes controlling flavivirus infection. Nat Microbiol. 2019 Dec;4(12):2369-2382.
11. Zhang S, Huang W, Ren L, et al. Comparison of viral RNA-host protein interactomes across pathogenic RNA viruses informs rapid antiviral drug discovery for SARS-CoV-2. Cell Res. 2022 Jan;32(1):9-23.
12. Gao G, Guo X, Goff SP. Inhibition of retroviral RNA production by ZAP, a CCCH-type zinc finger protein. Science (New York, NY). 2002;297:1703-6.
13. Bick MJ, Carroll JW, Gao G, et al. Expression of the zinc-finger antiviral protein inhibits alphavirus replication. J Virol. 2003 Nov;77(21):11555-62.
14. Nguyen LP, Aldana KS, Yang E, et al. Alphavirus Evasion of Zinc Finger Antiviral Protein (ZAP) Correlates with CpG Suppression in a Specific Viral nsP2 Gene Sequence. Viruses. 2023 Mar 24;15(4).
15. Liu CH, Zhou L, Chen G, et al. Battle between influenza A virus and a newly identified antiviral activity of the PARP-containing ZAPL protein. Proc Natl Acad Sci U S A. 2015 Nov 10;112(45):14048-53.
16. Mao R, Nie H, Cai D, et al. Inhibition of hepatitis B virus replication by the host zinc finger antiviral protein. PLoS Pathog. 2013;9(7):e1003494.
17. Muller S, Moller P, Bick MJ, et al. Inhibition of filovirus replication by the zinc finger antiviral protein. J Virol. 2007 Mar;81(5):2391-400.
18. Tang Q, Wang X, Gao G. The Short Form of the Zinc Finger Antiviral Protein Inhibits Influenza A Virus Protein Expression and Is Antagonized by the Virus-Encoded NS1. J Virol. 2017 Jan 15;91(2).

19. Zhu Y, Chen G, Lv F, et al. Zinc-finger antiviral protein inhibits HIV-1 infection by selectively targeting multiply spliced viral mRNAs for degradation. Proc Natl Acad Sci U S A. 2011 Sep 20;108(38):15834-9.

20. Takata MA, Goncalves-Carneiro D, Zang TM, et al. CG dinucleotide suppression enables antiviral defence targeting non-self RNA. Nature. 2017 Oct 5;550(7674):124-127.

21. Miyazato P, Matsuo M, Tan BJY, et al. HTLV-1 contains a high CG dinucleotide content and is susceptible to the host antiviral protein ZAP. Retrovirology. 2019 Dec 16;16(1):38.

22. Gonzalez-Perez AC, Stempel M, Wyler E, et al. The Zinc Finger Antiviral Protein ZAP Restricts Human Cytomegalovirus and Selectively Binds and Destabilizes Viral UL4/UL5 Transcripts. mBio. 2021 May 4;12(3).

23. Zhao Y, Song Z, Bai J, et al. ZAP, a CCCH-Type Zinc Finger Protein, Inhibits Porcine Reproductive and Respiratory Syndrome Virus Replication and Interacts with Viral Nsp9. J Virol. 2019 May 15;93(10).

24. Li MMH, Aguilar EG, Michailidis E, et al. Characterization of Novel Splice Variants of Zinc Finger Antiviral Protein (ZAP). J Virol. 2019 Sep 15;93(18).

25. Verschueren E, Von Dollen J, Cimermancic P, et al. Scoring Large-Scale Affinity Purification Mass Spectrometry Datasets with MiST. Curr Protoc Bioinformatics. 2015 Mar 9;49:8 19 1-8 19 16.

26. Jager S, Cimermancic P, Gulbahce N, et al. Global landscape of HIV-human protein complexes. Nature. 2011 Dec 21;481(7381):365-70.

27. Goodier JL, Pereira GC, Cheung LE, et al. The Broad-Spectrum Antiviral Protein ZAP Restricts Human Retrotransposition. PLOS Genetics. 2015;11:e1005252.

28. Ficarelli M, Neil SJD, Swanson CM. Targeted Restriction of Viral Gene Expression and Replication by the ZAP Antiviral System. Annu Rev Virol. 2021 Sep 29;8(1):265-283.

29. Caudron-Herger M, Rusin SF, Adamo ME, et al. R-DeeP: Proteome-wide and Quantitative Identification of RNA-Dependent Proteins by Density Gradient Ultracentrifugation. Mol Cell. 2019 Jul 11;75(1):184-199 e10.

30. Huttlin EL, Bruckner RJ, Paulo JA, et al. Architecture of the human interactome defines protein communities and disease networks. Nature. 2017 May 25;545(7655):505-509.

31. Youn JY, Dunham WH, Hong SJ, et al. High-Density Proximity Mapping Reveals the Subcellular Organization of mRNA-Associated Granules and Bodies. Mol Cell. 2018 Feb 1;69(3):517-532 e11.

32. Xu S, Ci Y, Wang L, et al. Zika virus NS3 is a canonical RNA helicase stimulated by NS5 RNA polymerase. Nucleic Acids Res. 2019 Sep 19;47(16):8693-8707.

33. Luo X, Wang X, Gao Y, et al. Molecular Mechanism of RNA Recognition by Zinc-Finger Antiviral Protein. Cell Rep. 2020 Jan 7;30(1):46-52 e4.

34. Zhang Z, Kim T, Bao M, et al. DDX1, DDX21, and DHX36 helicases form a complex with the adaptor molecule TRIF to sense dsRNA in dendritic cells. Immunity. 2011 Jun 24;34(6):866-78.

35. Kim T, Pazhoor S, Bao M, et al. Aspartate-glutamate-alanine-histidine box motif (DEAH)/RNA helicase A helicases sense microbial DNA in human plasmacytoid dendritic cells. Proc Natl Acad Sci U S A. 2010 Aug 24;107(34):15181-6.

36. Zhang Z, Yuan B, Lu N, et al. DHX9 pairs with IPS-1 to sense double-stranded RNA in myeloid dendritic cells. J Immunol. 2011 Nov 1;187(9):4501-8.

37. Pattabhi S, Knoll ML, Gale M, Jr., et al. DHX15 Is a Coreceptor for RLR Signaling That Promotes Antiviral Defense Against RNA Virus Infection. J Interferon Cytokine Res. 2019 Jun;39(6):331-346.

38. Miyashita M, Oshiumi H, Matsumoto M, et al. DDX60, a DEXD/H box helicase, is a novel antiviral factor promoting RIG-I-like receptor-mediated signaling. Mol Cell Biol. 2011 Sep;31(18):3802-19.

39. Ermler ME, Yerukhim E, Schriewer J, et al. RNA helicase signaling is critical for type i interferon production and protection against Rift Valley fever virus during mucosal challenge. J Virol. 2013 May;87(9):4846-60.

40. Steimer L, Klostermeier D. RNA helicases in infection and disease. RNA Biol. 2012 Jun;9(6):751-71.

41. Wu CY, Nagy PD. Role reversal of functional identity in host factors: Dissecting features affecting pro-viral versus antiviral functions of cellular DEAD-box helicases in tombusvirus replication. PLoS Pathog. 2020 Oct;16(10):e1008990.

42. Cheng W, Chen G, Jia H, et al. DDX5 RNA Helicases: Emerging Roles in Viral Infection. Int J Mol Sci. 2018 Apr 9;19(4).

43. Mitoma H, Hanabuchi S, Kim T, et al. The DHX33 RNA helicase senses cytosolic RNA and activates the NLRP3 inflammasome. Immunity. 2013 Jul 25;39(1):123-35.

44. Zhang Z, Yuan B, Bao M, et al. The helicase DDX41 senses intracellular DNA mediated by the adaptor STING in dendritic cells. Nat Immunol. 2011 Sep 4;12(10):959-65.

45. Chen G, Guo X, Lv F, et al. p72 DEAD box RNA helicase is required for optimal function of the zinc-finger antiviral protein. Proc Natl Acad Sci U S A. 2008 Mar 18;105(11):4352-7.

46. Ye P, Liu S, Zhu Y, et al. DEXH-Box protein DHX30 is required for optimal function of the zinc-finger antiviral protein. Protein Cell. 2010 Oct;1(10):956-64.

47. Zhu Y, Gao G. ZAP-mediated mRNA degradation. RNA Biol. 2008 Apr-Jun;5(2):65-7.

48. Chiu HP, Chiu H, Yang CF, et al. Inhibition of Japanese encephalitis virus infection by the host zinc-finger antiviral protein. PLoS Pathogens. 2018;14.

49. Li MM, Lau Z, Cheung P, et al. TRIM25 Enhances the Antiviral Action of Zinc-Finger Antiviral Protein (ZAP). PLoS Pathog. 2017 Jan;13(1):e1006145.

50. Zheng X, Wang X, Tu F, et al. TRIM25 Is Required for the Antiviral Activity of Zinc Finger Antiviral Protein. Journal of virology. 2017;91.

51. Ficarelli M, Wilson H, Pedro Galão R, et al. KHNYN is essential for the zinc finger antiviral protein (ZAP) to restrict HIV-1 containing clustered CpG dinucleotides. eLife. 2019;8.

52. Buckmaster MV, Goff SP. Riplet Binds the Zinc Finger Antiviral Protein (ZAP) and Augments ZAP-Mediated Restriction of HIV-1. Journal of Virology. 2022;96.

53. McDougal MB, De Maria AM, Ohlson MB, et al. Interferon inhibits a model RNA virus via a limited set of inducible effector genes. EMBO Rep. 2023 Sep 6;24(9):e56901.

54. Pallett MA, Lu Y, Smith GL. DDX50 Is a Viral Restriction Factor That Enhances IRF3 Activation. Viruses. 2022 Feb 3;14(2).

55. Buechler CR, Bailey AL, Weiler AM, et al. Seroprevalence of Zika Virus in Wild African Green Monkeys and Baboons. mSphere. 2017 Mar-Apr;2(2).

56. Kerns JA, Emerman M, Malik HS. Positive selection and increased antiviral activity associated with the PARP-containing isoform of human zinc-finger antiviral protein. PLoS Genet. 2008 Jan;4(1):e21.

57. Goncalves-Carneiro D, Takata MA, Ong H, et al. Origin and evolution of the zinc finger antiviral protein. PLoS Pathog. 2021 Apr;17(4):e1009545.

FIGURES

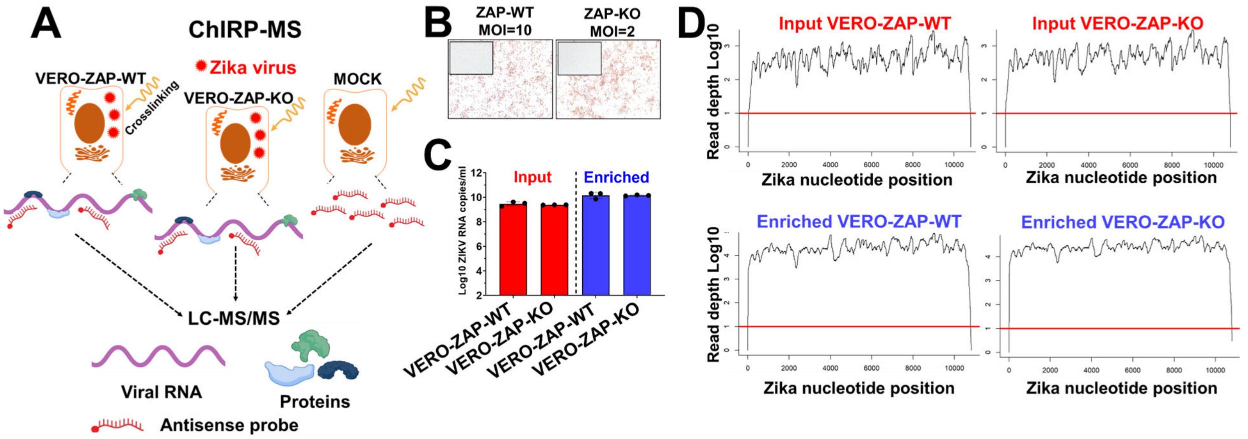

Fig 1. ChIRP-MS study design and validation. (A) ChIRP-MS experimental design to compare viral RNA–host protein interactions in ZAP-positive and ZAP-KO cells. ChIRP-MS was done in three biological replicates; each biological replicate consisted of lysed cells from four T-175 flasks for each experimental condition. **(B)** We adapted normalized MOIs to induce similar Zika viral loads in ZAP-WT and ZAP-KO cells. Red staining represents a similar number of Zika virus E protein-positive cells in WT and KO cells. Inserts—mock-infected cells. **(C)** The same Zika RNA loads in ZAP-WT and ZAP-KO cells were also confirmed using RT-qPCR. **Input** - sonicated cellular lysates. **Enriched** - immunoprecipitated viral RNA-protein complexes bound to MyOne C1 magnetic beads at the last washing step before protein elution. RNA was extracted from a 40 ul of cell lysate or bead suspension in the washing buffer representing each biological replicate and subjected to Zika virus-specific RT-qPCR; dots represent ChIRP-MS biological replicates. **(D)** The same nearly entire Zika RNA genome coverage and NGS depth in ZAP-WT and ZAP-KO cells. Representative data from one ChIRP-MS biological replicate for ZAP-WT and ZAP-KO cells. **Input** and **Enriched** are the same sample types as for RT-qPCR in **C**. Control NGS in mock-infected cells did not show Zika-specific sequences (not shown). A red line shows the 10-nucleotide NGS depth threshold.

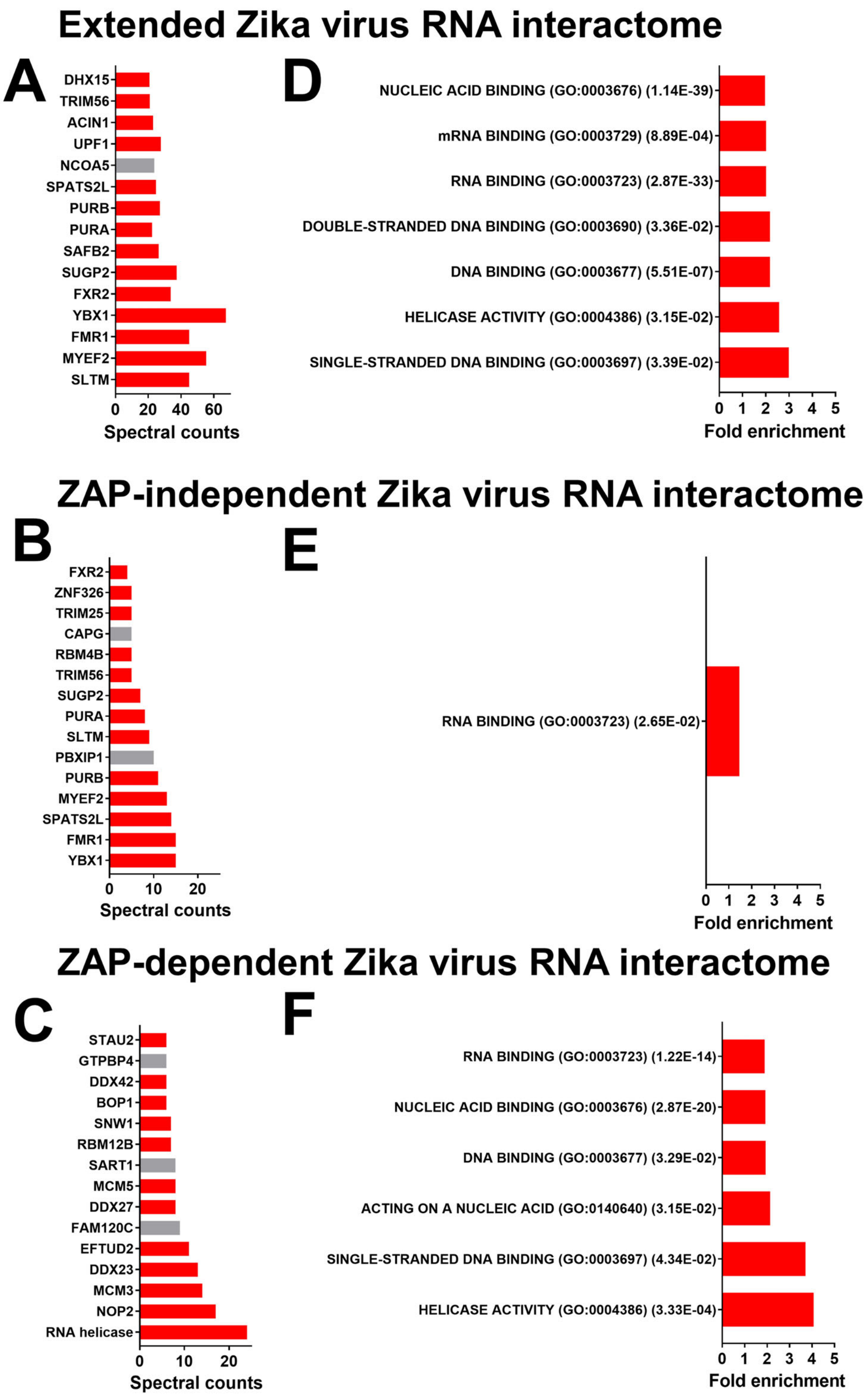

Fig 2. Top ChIRP-MS proteins and GO pathways identified in the Extended, ZAP-independent, and ZAP-dependent Zika virus RNA interactomes. Mean spectral counts are shown for proteins in (**A**, **B**, **C**). Spectral counts for all three biological replicates are shown in **Tables S2C, F, H**. The top proteins with unknown functions in RNA biology are highlighted in grey. For GO pathways in (**D, E, F**), GO identification numbers and FDR-adjusted *P* values are shown in parentheses. All GO processes were overrepresented.

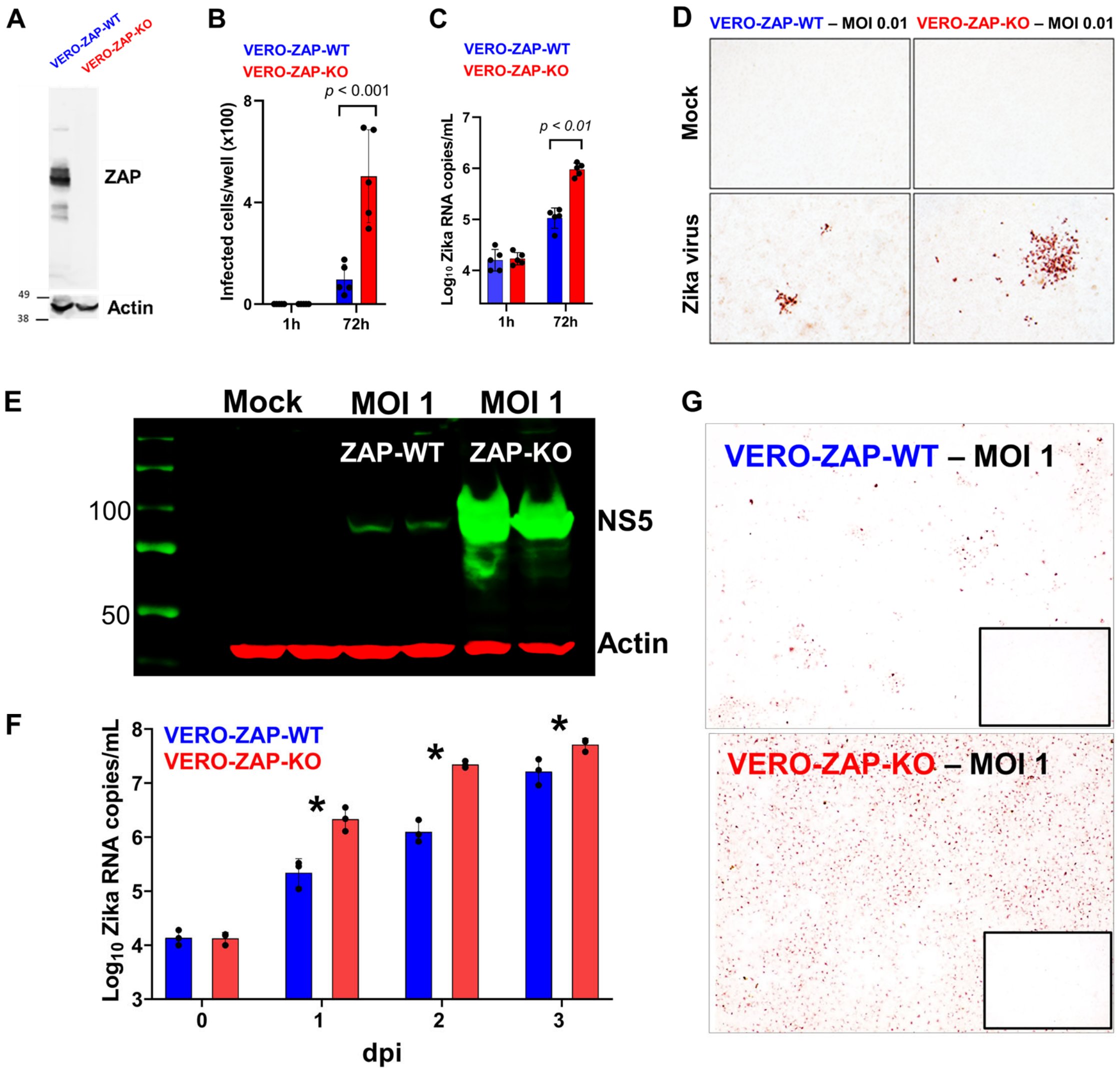

Fig 3. Infection phenotypes of Zika virus in wild-type (VERO-ZAP-WT) and ZAP knock-out (VERO-ZAP-KO) cells. (**A**) ZAP western blot. KO status was also confirmed by Sanger sequencing. (**B** and **C**) Reduced Zika virus infection in VERO-ZAP-WT cells at 72 h, MOI 0.01. Statistics—an unpaired t-test. The detection limit for RT-qPCR is 2.96 Log$_{10}$ of Zika virus RNA per 1 ml of supernatant. (**D**) Representative images of cells positive for Zika virus E protein (red staining) at 72 h, MOI 0.01. Magnification x200. The quantitative data are represented in **B**. The experiment was done in five replicates. Figures represent the general patterns in all replicates. (**E**) Reduced Zika virus infection in VERO-ZAP-WT cells at 72 h defined by western blot for Zika virus NS5 protein. Normalized 50 µg of protein was used for all samples. Two biological replicates for each condition are shown. (**F**) Zika virus RNA loads, MOI 1. *Unpaired t-test: $P = 0.0005$-0.03. All mock-infected samples were negative in Zika-specific RT-qPCR. The detection limit for RT-qPCR is 2.96 Log$_{10}$ of Zika virus RNA per 1 ml of supernatant. **dpi**: days post-infection. (**G**) Representative images of cells positive for Zika virus E protein (red staining) at 72 h, MOI 1. Magnification x100. Inserts are mock-infected cells. The experiment was done in three biological replicates. Figures represent the general patterns in all replicates. In these experimental conditions, Zika virus caused intensive diffuse infection with many positive VERO-ZAP-WT cells; but many cells were virus-negative. In VERO-ZAP-KO cells, Zika virus caused superinfection with almost all cells positive for viral E protein.

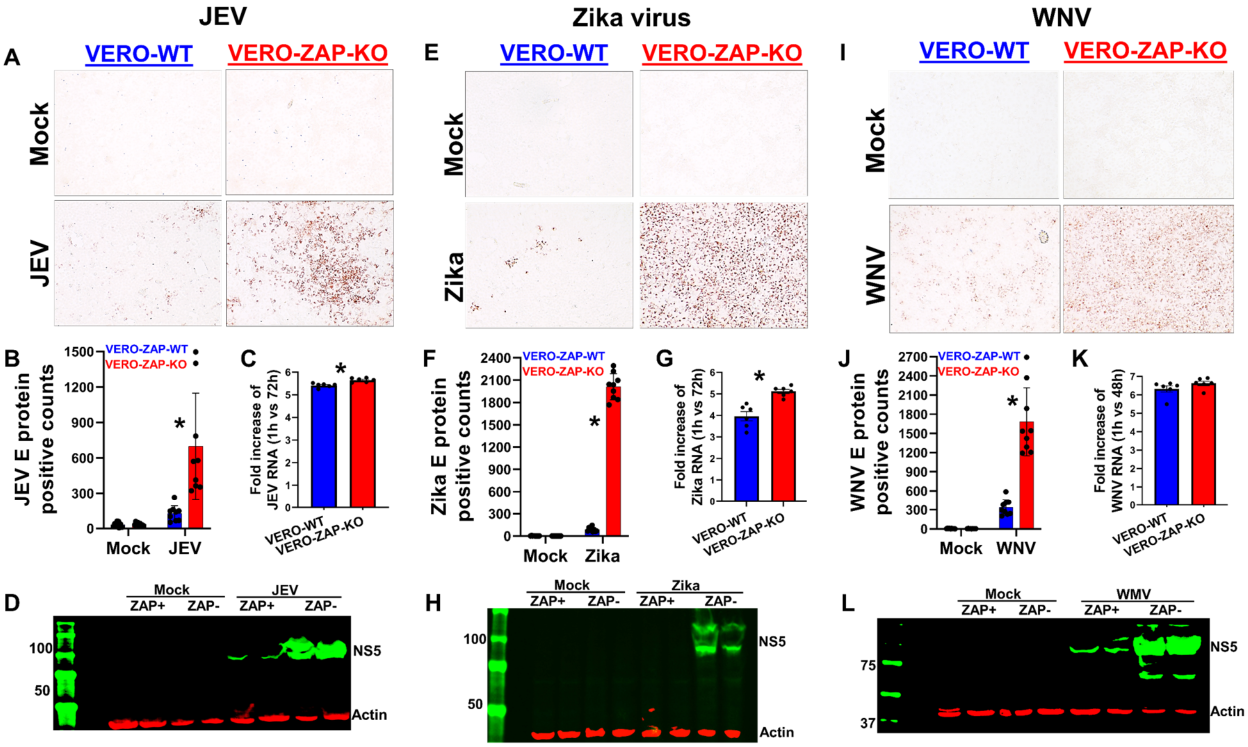

Fig 4. ZAP affects JEV, Zika, and WNV infection phenotypes. Representative images of cells positive for JEV (**A**), Zika virus (**E**), and WMV (**I**) E protein (red staining) at 72 h (48 h for WNV), MOI 0.01. Magnification x100. The experiment was done in 3 biological and 3 technical replicates. Figures represent the general patterns in all replicates. All 9 replicates for VERO-ZAP-WT and VERO-ZAP-KO cells are shown in **S1 Fig**. The digital quantification of JEV (**B**), Zika (**F**), and WNV (**J**) positive cells in all 9 replicates from **S1 Fig**. *Unpaired t-test: $P < 0.05$. In mock-infected cells digital sensitive counting represents the staining background. The fold increase of JEV (**C**), Zika (**G**), and WNV (**K**) RNA loads in cell lysates collected at 1 h and 72 h (48 h for WNV) after inoculation. VERO-WT and VERO-ZAP-KO cells were inoculated with MOI 0.01. Virus inoculums were removed and replaced with media. Cell lysates were collected with a lysis buffer at 1 h post-inoculation (to normalize for leftover virus inoculum RNA) and at 48-72 h. *Unpaired t-test: $P < 0.05$. The experiment was done in 3 biological and 2 technical replicates. (**D**, **H**, **L**) Reduced flavivirus infection in VERO-ZAP-WT cells at 72 h (48 h for WNV) represented by western blot for NS5 proteins. Normalized 50 μg of protein was used for all samples. Two biological replicates for each condition are shown.

SUPPORTING INFORMATION CAPTIONS

S1Fig. Representative images of cells positive for flavivirus E protein (red staining) at 72 h (JEV and Zika virus) and 48 h (WMV). The experiment was done in 3 biological and 3 technical replicates. All replicates are shown. MOI 0.01. The data from these replicate figures were used for digital quantification in **Figs 4B**, **F**, **J**. (**A**) JEV in VERO-ZAP-WT cells. (**B**) JEV in VERO-ZAP-KO cells. (**C**) Zika virus in VERO-ZAP-WT cells. (**D**) Zika virus in VERO-ZAP-KO cells. (**E**) WNV in VERO-ZAP-WT cells. (**F**) WNV in VERO-ZAP-KO cells.

Table S1 - ChIRP-MS data.

SUPPLEMENTAL MATERIALS AND METHODS

Endogenous ZAP affects Zika virus RNA interactome

Ahmad Jawad Sabir[1,a], Nguyen Phuong Khanh Le[2,a], Prince Pal Singh[2,3,a], Uladzimir Karniychuk[2,*]

[1]Department of Microbiology and Immunology, University of Illinois, College of Medicine, Chicago, IL, USA

[2]Department of Veterinary Biosciences, College of Veterinary Medicine, The Ohio State University, Columbus, OH, USA

[3]School of Public Health, University of Saskatchewan, Saskatoon, Canada

[a]: These authors contributed equally

*** Correspondence:** Uladzimir Karniychuk
Department of Veterinary Biosciences, College of Veterinary Medicine, The Ohio State University, Columbus, OH, USA
karniychuk.1@osu.edu

SUPPLEMENTAL MATERIALS AND METHODS

Cells

Wild-type VERO E6 cells (ATCC) (VERO-ZAP-WT) and ZAP-KO derivatives (VERO-ZAP-KO) were maintained in DMEM supplemented with 10% heat-inactivated fetal bovine serum (FBS), 1x Penicillin-Streptomycin, and 2.67 mM sodium bicarbonate at +37°C in a 5% CO_2 humidified incubator. To generate Zinc finger CCCH-type antiviral protein 1 (ZAP) KO cell line, the guide RNA (gRNA) GTCTCTGGCAGTACTTGCGA which targets the *Chlorocebus sabaeus* (Gene ID: 103226990) ZC3HAV1 sequence was used. A non-targeting control gRNA ACGGAGGCTAAGCGTCGCAA was also used. gRNA was transiently transfected into cells using GenCrispr NLS-Cas9-NLS Nuclease (GenScript). Transfected cells were plated in 96-well plates by limiting dilution to generate isogenic single clones. The clones were expanded and genotyped with Sanger sequencing; primers (F-ATCGCTGGGCTGGACTAACG, R-GCAGAGAAGGGAGTGGCTGAA) were used to identify indels. The knock-out subclone verified by genotyping was further confirmed by western blot for ZAP expression as described below. Free mycoplasma contamination status in cells was confirmed using the LookOut Mycoplasma PCR Detection Kit (Millipore Sigma).

Viruses

We used the Asian lineage Zika virus H/PF/2013 strain. Zika virus was synthetically rescued with reverse genetics in our previous study [1]; H/PF/2013 [GenBank: KJ776791.2] reference sequence was used to rescue the virus. For JEV (SA14-14-2 strain, GenBank MK585066.1) and WNV (NY99 strain, GenBank: DQ211652.1), we used the same reverse genetics system [1].

Viruses were propagated in VERO cells in DMEM supplemented with 2% FBS and 1% penicillin/streptomycin (P/S). Supernatants were centrifuged (12,000 g, 20 min, +4°C), aliquoted, and frozen (-80°C). Infectious virus titers were quantified using VERO E6 cells with the endpoint dilution assay, and fifty percent tissue culture infective dose ($TCID_{50}$) endpoint titers were calculated as previously described [1-4]. Media from virus-negative VERO cells was processed in the same manner and used in control conditions. Free mycoplasma contamination status in virus stocks was confirmed using the LookOut Mycoplasma PCR Detection Kit (Millipore Sigma).

Comprehensive Identification of RNA binding Proteins by Mass Spectrometry (ChIRP-MS)

We performed ChIRP-MS as described before [5-8]. Biotinylated DNA probes (**Table S2A**) covering the whole Zika virus genome were designed using the online tool (https://www.biosearchtech.com/support/tools/design-software/chirp-probe-designer). To have an even coverage of the whole genome, 50 probes were designed by dividing the whole Zika reference sequence H/PF/2013 [GenBank: KJ776791.2] into two segments (1-5400 and 5401-10807), with a repeat masking setting of 3 and spacing length of 80 (1 oligo around every 200 bp). Oligos were synthesized with 3' biotin-TEG modification, final yield of 2 OD, and HPLC purification at Bio Basic Inc Canada. Fifty individual oligos were resuspended at 100 µM and mixed at equal volumes to prepare probe pool.

For Zika virus infection, VERO-ZAP-WT and VERO-ZAP-KO cells were seeded at 10^7 cells per T-175 flask (4 flasks per experimental condition x 3 biological replicates) and were grown in DMEM supplemented with 10% FBS. The next day, the media was removed, and cell monolayers were washed with PBS and inoculated with Zika virus at MOI 10 for VERO-ZAP-WT cells and MOI 2 for VERO-ZAP-KO cells; these MOIs were adapted to provide the same Zika virus loads (see results for details). To exclude the effects of differential uptake of the stimulus with MOI 10 in VERO-ZAP-WT cells, during VERO-ZAP-KO MOI 2 Zika virus inoculation we added heat-inactivated virus equivalent of MOI 8. Control cells were mock-treated with supernatant from virus-free control cells. Flasks were incubated at 37°C for 2 h and gently shaken every 10 minutes. The inoculum from flasks was removed, and monolayers were extensively washed with 1× PBS twice and 25 mL of DMEM supplemented with 2% FBS was added to each flask. After 72 h, for cell harvesting and chemical crosslinking, media was removed, cell monolayers were rinsed with PBS, trypsinized, washed, and cells from four flasks representing one biological replicate were pooled for each experimental condition. Cells were cross-linked in 37 mL of 3% methanol free- formaldehyde (diluted in PBS) and incubated for 30 min at room temperature on a rotator. Afterwards, formaldehyde was quenched with 3.7 mL of 1.25 M glycine (final concentration 125 mM) and pelleted (2,000g, 5 min, +4°C). Cell pellets were washed, resuspended in 2. 5ml of PBS, transferred to pre-weighed microcentrifuge tubes, and centrifuged (10,000g, 2 min, +4°C). PBS was aspirated, tubes were placed on ice and weighted on an analytical scale to determine the final pellet weight, snap frozen in liquid nitrogen, and stored at -80°C. Around 300 mg of cells was obtained from four T-175 flasks.

For cell lysis and sonication, cell pellets were thawed at RT, resuspended in the ChIRP lysis buffer (50 mM Tris-HCl, pH 7.0, 10 mM EDTA, 1% SDS) supplemented just before use with PMSF (100 mM; Fisher; 10 µl per 1 ml of ChIRP lysis buffer), SUPERaseIn (20 U/ µl; Fisher; 10 ul per 1 ml of ChIRP lysis buffer), and protease inhibitor (100x; Fisher #P178410; 10 ul per 1 ml of ChIRP lysis buffer) to finally have 300 mg of cell pellet per 4 ml of the complete lysis buffer. The lysate from each sample were aliquoted in 2 ml and sonicated using Sonics Ultrasonic Processor VCX750 with 3 mm microtip at 20% amplitude with 15 seconds On, 45 seconds Off pulse intervals for 1 h (1 h for total 15 + 45 seconds On and Off intervals) in 15 mL MI Bioruptor Plus TPX Tubes. The sonicated lysates were snap frozen in liquid nitrogen and stored at -80°C until further use. Aliquots of sonicated lysates (40 µL) were used to extract RNA/DNA with the Invitroge PureLink RNA Mini Kit according to manufacturer's instructions, and the efficiency of sonication was confirmed by running extracts from all samples on 1% agarose gels. The average DNA/RNA length was around 500 nucleotides in all samples. The RNA from these samples were also used for Zika-specific RT-qPCR and Next Generation Sequencing (NGS) to analyze the entire Zika virus RNA loads, genome coverage and NGS depth (see below and results).

For hybridization, sonicated lysates were thawed on ice and pre-cleaned by adding 30 µL washed Invitrogen Dynabeads MyOne Streptavidin C1 (Fisher # 65001) per 1 mL of lysate and rotating at 37°C for 30 min in a hybridization oven. Beads were removed twice from lysates using a magnetic stand; for this and all subsequent magnetic stand steps > 2 min magnetization was applied before removing supernatant. Next, for every 1 mL of pre-cleaned sonicated lysate, 2 mL of ChIRP hybridization buffer (750 mM NaCl, 1% SDS, 50 mM Tris-HCl pH 7.0, 1 mM EDTA, 15% formamide supplemented with PMSF, SUPERaseIn, and protease inhibitor as described above for lysis buffer) and 2.5 µL of the 100 µM ChIRP probe pool were added. In our experiments, the total volume of pre-cleaned sonicated lysate and ChIRP hybridization buffer was 12 ml per sample; for efficient hybridization, we distributed each sample in 6 ml aliquots and rotated in the hybridization over for 16 h at 37°C.

For enrichment of hybridized Zika virus RNA and associated proteins, per 1 mL of initial sample, 250 µL of washed (washed 3 times in un-supplemented lysis buffer) Dynabeads MyOne Streptavidin C1 was added in each sample (in our study 1 ml of beads was added per initial 4 ml lysis buffer sample), and rotated in the hybridization oven for 45 min at 37°C. Two 15 ml tubes representing one sample were placed on the magnetic stand, supernatants were removed, and beads were combined in 1 ml of ChIRP wash buffe (2x SSC, 0.5% SDS supplemented with 1 mM PMSF just before use) in 1.5 ml low-binding Eppendorf tube. Afterward, beads were washed 5 times in 1 ml of the ChIRP wash buffer by rotating at 37°C for 5 min in the hybridization over, placing for 4 min on the magnetic stand, and replacing the wash buffer. During the final wash, 10 µL of beads in the wash buffer were collected for RNA extraction, Zika-specific RT-qPCR and NGS to analyze the Zika RNA loads, entire virus genome coverage and NGS depth (see below and results).

For elution, beads were collected on the magnetic stand, resuspended in 600 µL of the ChIRP biotin elution buffer (12.5 mM biotin, 7.5 mM HEPES, pH 7.9, 75 mM NaCl, 1.5 mM EDTA, 0.15% SDS, 0.075% sarkosyl, and 0.02% Sodium deoxycholate), rotated at 25°C for 20 min, and at 65°C for 15 min. Beads were placed on the magnetic stand and eluents were transferred to a fresh tube, and beads were eluted again with 600 µL of the ChIRP biotin elution buffer. The two eluents were pooled (final 1200 µL) and residual beads were removed again using the magnetic stand. Afterward, 300 µL of trichloroacetic acid (25% of the final elute volume) was added to the clean eluent, vortexed, and placed at 4°C overnight for precipitation. The next day, proteins were pelleted at 21,000 g at 4°C for 45 min. Supernatants were carefully removed, and protein pellets were washed once with ice-cold acetone. Samples were span at 21,000 g at 4°C for 5 min. Acetone was removed, tubes briefly centrifuged again and after removal of residual acetone were left to air-dry for 1 minute. Then, 60 µL of preheated 1× ChIRP lysis buffer containing 50 mM TEAB (Fisher # PI90114) and 5% SDS (Fisher # BP2436-200) were added to the protein pellet and gently mixed several times with 200 µL pipette tips. Samples were immediately put on dry ice and stored in -80°C until sent to the proteomics facility.

To validate the same viral RNA loads in all samples/experimental conditions at the time of formaldehyde RNA-protein fixation and ChIRP, RNA extracted during cell lysis (input) and elution steps (enriched) (see above) were tested with Zika virus-specific RT-qPCR assay and NGS to analyze the entire Zika virus genome coverage and NGS depth. The Zika virus-specific RT-qPCR assay was conducted as described below. For NGS, samples were brought to the final volume of 50 µL with 1x PBS and 5 µL Proteinase K (Fisher) and incubated at 55˚C for 30 minutes. Then, RNA was extracted with the RNA Clean & Concentrator-5 Research Kit (ZYMO) and treated with the Invitrogen TURBO DNA-free Kit (Fisher). Afterward, 7 µL of RNA was used to produce cDNA with the Maxima H Minus First Strand cDNA Synthesis Kit (Fisher) and random hexamers, following the manufacturer's instructions. The single stranded cDNA (20 µL) was further used to prepare double-stranded DNA (dsDNA) using the NEBNext® Second Strand Synthesis (dNTP-free) Reaction Buffer (NEB #B6117S) mixed with the DNA Polymerase I (NEB #M0209S), E. coli DNA Ligase (NEB #M0205S), RNase H (NEB, #M0297S), random hexamers, and dNTPs mix. The dsDNA was used for library construction with the NEBNext® Ultra II DNA Library Prep Kit for Illumina (NEB #E7645L) and NEBNext® Multiplex Oligos for Illumina® (96 Index Primers) (NEB #E6609S) as we previously described [9-11]. Briefly, the libraries were constructed according to the manufacturer's instructions, with 1:10 adaptor dilution (volume of adaptor:total volume), and following cleanup step of adaptor-ligated DNA without size selection. Individual libraries were quantified using Qubit dsDNA HS Assay Kit (FisherScientific) and Qubit 4.0 Fluorometer (Fisher). The peak size of the libraries was confirmed with the Agilent DNA 1,000 kit on Agilent 2100 Bioanalyzer (Agilent). Afterward, 20 ng of each barcoded library were pooled, quantified (Qubit), quality-checked (Agilent Bioanalyzer), and converted to moles: Molecular weight [nM] = Library concentration [ng/µL] / (Average library size x 650)/1,000,000). The pooled library was diluted to 2 nM in 10 mM TE buffer, denatured with 0.1 N NaOH, diluted to 14 pM, and paired-end 300 nt reads were generated with the MiSeq Reagent kit v3 (600 cycle output; Illumina) on the MiSeq System (Illumina). To compare Zika virus RNA coverage and NGS depth, FASTQ files representing different samples/experimental conditions were trimmed for adaptor sequences and filtered for low-quality reads using Trimmomatic. Next, the trimmed FASTQ paired files were aligned to the Zika virus reference sequence H/PF/2013 [GenBank: KJ776791.2] using Burrows-Wheeler Aligner (BWA) [12] and output BAM files were used to quantify and visualize the virus genome coverage and NGS depth with the in-house R script [9-11].

Preparation and mass spectrometry analysis of ChIRP samples were done in The Proteomics Facility, Network Biology Collaborative Centre, Lunenfeld-Tanenbaum Research Institute, Toronto. For the S-Trap (ProtiFi) [13,14] the whole volume containing ChIRP-precipitated proteins were used. The material was reduced with 20 mM DTT for 10 minutes at +95°C and alkylated with 40 mM iodoacetamide for 30 minutes in the dark. Phosphoric acid was added to achieve a final concentration of 1.2%. To each 27.5 µl of acidified lysate, 165 µl of S-Trap protein binding buffer (90% methanol, 100 mM TEAB) was added. The resulting mixture was passed through the micro column at 4,000 × g, and the column was washed four times with the S-Trap protein binding buffer. Each sample was digested with 1 µg of trypsin (in 20 µl of 50 mM TEAB) for 1 hour at +47°C. Prior to elution, 40 µl of 50 mM TEAB (pH 8) was added to the column. Peptides were eluted by centrifugation at 4,000 × g. Peptides were eluted two more times with 40 µl of 2% formic acid and 40 µl of 50% acetonitrile + 2% formic acid. Eluted peptides were dried down and stored at -40°C.

For data-dependent acquisition (DDA) LC-MS/MS, digested peptides were analyzed using a nano-HPLC coupled to MS. Half of the sample was used for DDA. Coated Nano-spray emitters were generated from fused silica capillary tubing, with 75µm internal diameter, 365µm outer diameter and 5-8µm tip opening, using a laser puller (Sutter Instrument Co., model P-2000, with parameters set as heat: 280, FIL = 0, VEL = 18, DEL = 2000). Nano-spray emitters were packed with C18 reversed-phase material (Reprosil-Pur 120 C18-AQ, 1.9 µm) resuspended in methanol using a pressure injection cell. The sample in 5% formic acid was directly loaded at 400 nl/min onto a 75 µm x 15 cm nano-spray emitter. Peptides were eluted from the column with an acetonitrile gradient generated by an Vanquish Neo UHPLC System and analyzed on an Orbitrap Fusion Lumos Tribrid. The gradient was delivered at 200 nl/min from 3.2% acetonitrile with 0.1% formic acid to 35.2% acetonitrile with 0.1% formic acid using a linear gradient of 90 minutes. This was followed by a 3 min gradient from 35.2% acetonitrile with 0.1% formic acid to 79.2% acetonitrile with 0.1% formic acid. After, there was a 5.8 min wash with 79.2% acetonitrile with 0.1% formic acid, and the column was equilibrated at 400nl/min for 6.4min. The total DDA protocol was 99 minutes. The MS1 scan had an accumulation time of 50 ms within a mass range of 400–1500Da, using orbitrap resolution of 120000, 60% RF lens, AGC target of 125% and 2400 volts. This was followed by MS/MS scans with a total cycle time of 3 seconds. Accumulation time of 50 ms and 33% HCD collision energy was used for each MS/MS scan. Each candidate ion was required to have a charge state from 2-7 and an AGC target of 400%, isolated using orbitrap resolution of 15,000. Previously analyzed candidate ions were dynamically excluded for 9 seconds.

Mass spectrometry RAW data files were converted using ThermoRawFileParser GUI -V 1.7.1 (https://github.com/compomics/ThermoRawFileParserGUI) to the mzML format compatible with FragPipe. The RAW files were analyzed using FragPipe v18.0, which utilized MSFragger v3.5, Philosopher v4.4.0, and IonQuant for peptide searching in the raw files [15-17]. The LFQ-MBR workflow was used, with the *Chlorocebus sabaeus* Proteome ID UP000029965 (https://www.uniprot.org/proteomes/UP000029965) database with appended Zika virus H/PF/2013 [GenBank: KJ776791.2], decoys, and contaminants sequences. Data from the output "combined_protein.tsv" file (**Table S1B**) were used for interactome analysis described below.

Identification of Extended, ZAP-independent, and ZAP-dependent Zika virus RNA interactomes from ChIRP-MS results

The Zika virus RNA-interacting proteins were scored with the Mass spectrometry interaction STatistics (MiST) analysis which was previously applied for ChIRP-MS [8,18,19]. We used MiST default parameters; for specificity, we also selected the Singleton Filtering MiST option to exclude proteins with spectral counts in only one biological replicate and quantify proteins with MiST score 0.75 or above [8,18,19]. We also excluded all proteins which had at least a single spectral count in at least one of biological replicate in mock-infected wild-type or ZAP-KO cells. We applied three analytical strategies to examine ChIRP-MS data. For the first analytical strategy, using the raw ChIRP-MS data with total 2,269 proteins (**Table S1B)**, we identified proteins specifically associated with Zika virus RNA in VERO-ZAP-WT cells. We defined the resultant list of enriched proteins as “extended” Zika virus RNA interactome in VERO-ZAP-WT cells. For the second analytical strategy, we identified proteins specifically interacting with Zika virus RNA in VERO-ZAP-KO cells. We defined the resultant list of enriched proteins as “ZAP-independent” Zika virus RNA interactome. We defined this interactome as ZAP-independent because associated cellular proteins were discovered in VERO-ZAP-KO cells which shows ZAP-independent nature of interactions. Finally, for the discovery of “ZAP-dependent” Zika RNA interactome in VERO-ZAP-WT cells, in addition to the above specificity exclusion criteria in MiST settings and in mock-infected cells, we excluded proteins which had at least one spectral count in at least one of the biological replicates in VERO-ZAP-KO cells infected with Zika virus.

For ZAP-independent and ZAP-dependent Zika virus RNA interactomes, we performed GO enrichment analyses of the identified proteins using The Gene Ontology Resource (https://geneontology.org/) which connects to the analysis tool from the PANTHER Classification System [20-22]. For analysis, GO aspect molecular function was selected. As recommended, a custom reference list containing all proteins’ IDs identified in the specific mass spectrometry run (**Tables S1B**) was added after initial analysis on The Gene Ontology Resource and the analysis was re-run on the PANTHER website. The significance *P* values of GO terms were calculated by Fisher’s exact test and adjusted by FDR.

Comparative infection phenotypes in wild-type and ZAP-KO cells infected with Zika virus, JEV, and WNV

ZAP-WT and ZAP-KO VERO cells were infected with Zika virus. Cells in suspension were inoculated at a multiplicity of infection (MOI) of 0.01 or 1 in 100 µL of DMEM for 1 h at 37°C and shaken gently every 10 minutes. The inoculum was removed and cells were washed with DMEM supplemented with 10% FBS and seeded in 24-well plates. Wells were prefilled with 900 µL of DMEM supplemented with 10% FBS and 100 µL of inoculated cells were added to get a resulting concentration of 2×10^5 cells per well with 3-5 replicates. Mock-infected cells were used as controls in each plate. Plates were incubated at 37°C and 5% CO_2. Afterwards, cell culture supernatants were collected at time points shown in figures, clarified (2,000 g, 10 min) and stored at −80°C for viral RNA copies quantification with virus-specific RT-qPCR [3,4,23,24]. The cell monolayers were air-dried, frozen (-80°C) and dried again before Zika virus antigen staining. Monolayers were formalin fixed and stained with virus-specific 4G2 (ATCC; HB-112) antibodies [1-4], and infected cells positive for Zika virus E protein were counted in each well with bright-field microscopy.

Next, we tested alongside JEV, Zika virus, and WNV in VERO-ZAP-WT and VERO-ZAP-KO cells. Fifty thousand cells per well were seeded into 96-well plates; next day, media was removed, and monolayers were inoculated with MOIs 0.01 of JEV, Zika, or WNV in 50 µl for 2 h at +37°C and 5% CO_2. Afterward, the inoculum was removed and replaced with 150 µl DMEM supplemented with 2% FBS, 1x Penicillin-Streptomycin, and 2.67 mM sodium bicarbonate. At 1 h and 72 h (48 h for WNV), cells in 9 wells representing three biological and three technical replicates were fixed and stained for flavivirus E protein as described above. For immunohistochemistry staining we used 4G2 (ATCC; HB-112) antibodies against Zika and WNV E protein, and GTX125867 (GeneTex) against JEV E protein. To quantify and compare immunohistochemistry staining between ZAP-WT and ZAP-KO conditions, a magnification x100 images were randomly acquired in all replicates with the same microscopic settings. Afterward each image was procced in ImageJ (NIH) with Automatic Particle counting (https://imagej.net/imaging/particle-analysis). In addition, cell lysates from 3 biological and 2 technical replicates were collected at the same time points with 140 µl of PureLink RNA Mini Kit lyses buffer (Invitrogen) for subsequent RNA extraction and virus-specific RT-qPCR. The difference between ZAP-WT and ZAP-KO conditions was represented by fold change of viral RNA loads in cell culture lysates collected at 1 h and 72 h (48 h for WNV) after inoculation (1 h after inoculation was used to normalize for leftover virus inoculum RNA).

RNA extraction and virus-specific reverse transcriptase quantitative polymerase chain reaction assays (RT-qPCR)

For extracellular RNA, we used QIAamp Viral RNA Mini Kit (QIAGEN) according to the manufacturer's instructions to purify Zika virus RNA from 140 µL of cell culture supernatants. For intracellular RNA, Zika virus, JEV, and WNV RNA was extracted from cell lysates with PureLink RNA Mini Kit (Invitrogen) according to the manufacturer's instructions. All RT-qPCR reactions were conducted on the QuantStudio 3 real-time PCR system (Applied Biosystems) and analyzed using QuantStudio Design & Analysis Software v1.5.2.

For Zika virus RNA quantification, we used the previously validated SYBR one-step RT-qPCR assay [25]. The Luna Universal One-Step RT-qPCR Kit (NEB) reaction mixture (20 µL) consisted of 10 µL Luna Universal One-Step Reaction Mix, 1 µL Luna WarmStart RT Enzyme

Mix, 1 µL (10 µM) of forward (ZIKV-F-SYBR: 5′-AGGATCATAGGTGATGAAGAAAAGT-3′) and reverse (ZIKV−R-SYBR: 5′-CCTGACAACACTAAGATTGGTGC-3′) primers, 3.4 µL nuclease-free water and 4 µL of RNA template. The reverse transcription and enzyme activation steps of 10 min at 55˚C and 1 min at 95˚C were followed by 40 amplification cycles (10 s at 95˚C and 60 s at 60˚C). A standard curve was generated using viral RNA, T7 promoter sequence, MAXIscript™ T7 Transcription Kit (Invitrogen), TURBO DNase (Fisher) treatment, RNA Clean & Concentrator-5 kit (ZYMO) following Qubit RNA High Sensitivity (HS) Kit (Invitrogen) quantification, and was used to quantify Zika RNA loads as we described [1,3].

For JEV (F: 5′-GCCACCCAGGAGGTCCTT-3′; R: 5′-CCCCAAAACCGCAGGAAT-3′; Probe: 56-FAM-CAAGAGGTG/ZEN/GACGGCC-3IABkFQ) and WNV (F: 5′-AGTAGTTCGCCTGTGTGAGC-3′; R: 5′-GCCCTCCTGGTTTCTTAGA-3′; Probe: 5’-FAM-AATCCTCACAAACACTACTAAGTTTGTCA-TAMRA-3’) we used the previously validated probe-based one-step RT-qPCR assays [26,27]. The Luna Universal Probe One-Step RT-qPCR Kit (NEB) reaction mixture (20 µL) consisted of 10 µL Luna Universal Probe One-Step Reaction Mix, 1 µL Luna WarmStart RT Enzyme Mix, 1 µL (10 µM) of forward and reverse primers, 0.5 µL of the probe, 2.5 µL nuclease-free water and 4 µL of RNA template. The reverse transcription and enzyme activation steps of 10 min at 55˚C and 1 min at 95˚C were followed by 40 amplification cycles (10 s at 95˚C and 30 s at 60˚C). A standard curve was used to quantify viral RNA loads as we described [28].

PCR values were corrected for volumes (140 µl of supernatant or cell lyses buffer) and upon logarithmical transformation expressed as virus RNA genome copies per mL. Strict precautions were taken to prevent PCR contamination. All master mix preparations were done in the dedicated PCR cabinet. Aerosol-resistant filter pipette tips and disposable gloves were used. Kit reagent controls were included in every RNA extraction and PCR run.

Western blot

Cells in T-75 or T-175 flasks were washed, pelletized, and lysed in 150 or 300 µL of RIPA buffer (Fisher) supplemented with 1× Halt protease inhibitor cocktail (Fisher) and 1× EDTA (Fisher). After 10 minutes of incubation on wet ice, the suspension was gently vortexed and centrifuged (12,000g, 10 min, +4 °C). Supernatants were aliquoted in prechilled low protein binding tubes (Sarstedt) and stored at −80°C. After quantifying protein concentration with the Pierce BCA Protein Assay Kit (Fisher), 50 µg of protein extract was diluted in 4x reducing Laemmli SDS sample buffer (Fisher), boiled at 95ºC for 10 min, and resolved using a 10% Mini-PROTEAN TGX precast protein gels (Bio-Rad) running in 1X Tris/Glycine/SDS running buffer (Bio-Rad) at a constant current of 125V for 70 min. Proteins were transferred to methanol-activated 0.45 µm Immun-Blot Low Fluorescence polyvinylidene fluoride (PVDF) membranes using Trans-Blot Turbo RTA Mini 0.45µm LF PVDF Transfer Kit (Bio-Rad, Cat. 1704274). Afterward, PVDF membranes were blocked with 1X VWR Life Science Rapidblock™ Blocking Solution (VWR) for 1 h at room temperature. The blocked membranes were incubated with primary antibody diluted in blocking solution overnight at +4°C. Membranes were washed four times with TBST (1x Bio-Rad Tris Buffered Saline containing 0.1% of Fisher Tween-20). After that, membranes were incubated with secondary antibody along with hFAB™ Rhodamine Anti-Actin Primary Antibody (Recombinant human β-actin) diluted in Blocking Solution for 1 h at room temperature, and washed four times with TBST. Fluorescent blots were imaged on the

ChemiDoc MP Imaging system using an appropriate detection channel with Image Lab Touch Software (Bio-Rad).

We used antibodies (Abs): Rabbit anti-ZAP IgG Abs (1:1,000 dilution; ANTI-ZC3HAV1 HPA059096-100UL, Sigma-Aldrich), Rabbit anti-Zika virus NS5 IgG Abs (1:1,000 dilution; GTX133312, GeneTex), Rabbit anti-West Nile virus NS5 IgG Abs (1:1,500, GTX131961, GeneTex), Rabbit anti-Japanese Encephalitis virus NS5 Abs (1:1,500, GTX131359, GeneTex), hFAB™ Rhodamine Anti-Actin Primary Abs (1:2,500; #12004164, BIO-RAD), and IRDye® 680RD Goat anti-Rabbit IgG secondary Abs (1:10,000; 926-68071, LI-COR).

Statistics

We used GraphPad PRISM 9 software. For the comparison of the number of virus-positive cell counts and viral RNA loads between wild-type and ZAP-KO cells we used an unpaired t-test. *P*-value < 0.05 was considered statistically significant.

SUPPLEMENTAL REFERENCES

1. Trus I, Udenze D, Berube N, et al. CpG-Recoding in Zika Virus Genome Causes Host-Age-Dependent Attenuation of Infection With Protection Against Lethal Heterologous Challenge in Mice. Front Immunol. 2019;10:3077.
2. Trus I, Berube N, Jiang P, et al. Zika Virus with Increased CpG Dinucleotide Frequencies Shows Oncolytic Activity in Glioblastoma Stem Cells. Viruses: Multidisciplinary Digital Publishing Institute; 2020. p. 579.
3. Udenze D, Trus I, Berube N, et al. The African strain of Zika virus causes more severe in utero infection than Asian strain in a porcine fetal transmission model. Emerging Microbes & Infections. 2019; 8:1098-1107.2019.
4. Darbellay J, Cox B, Lai K, et al. Zika Virus Causes Persistent Infection in Porcine Conceptuses and may Impair Health in Offspring. EBioMedicine. 25:73-86.2017.
5. Chu C, Zhang QC, da Rocha ST, et al. Systematic discovery of Xist RNA binding proteins. Cell. 2015 Apr 9;161(2):404-16.
6. Flynn RA, Belk JA, Qi Y, et al. Discovery and functional interrogation of SARS-CoV-2 RNA-host protein interactions. Cell. 2021 Apr 29;184(9):2394-2411 e16.
7. Ooi YS, Majzoub K, Flynn RA, et al. An RNA-centric dissection of host complexes controlling flavivirus infection. Nat Microbiol. 2019 Dec;4(12):2369-2382.
8. Zhang S, Huang W, Ren L, et al. Comparison of viral RNA-host protein interactomes across pathogenic RNA viruses informs rapid antiviral drug discovery for SARS-CoV-2. Cell Res. 2022 Jan;32(1):9-23.
9. Sabir AJ, Singh PP, Trus I, et al. Asian Zika virus can acquire generic African-lineage mutations during in utero infection. Emerg Microbes Infect. 2023 Dec;12(2):2263592.
10. Udenze D, Trus I, Berube N, et al. CpG content in the Zika virus genome affects infection phenotypes in the adult brain and fetal lymph nodes. Front Immunol. 2022;13:943481.
11. Udenze D, Trus I, Munyanduki H, et al. The isolated in utero environment is conducive to the emergence of rna and dna virus variants. Viruses: Multidisciplinary Digital Publishing Institute; 2021. p. 1827.
12. Li H, Durbin R. Fast and accurate short read alignment with Burrows-Wheeler transform. Bioinformatics. 2009 Jul 15;25(14):1754-60.
13. Bang G, Lee H, Kim H, et al. Comparison of protein characterization using In solution and S-Trap digestion methods for proteomics. Biochem Biophys Res Commun. 2022 Jan 22;589:197-203.
14. HaileMariam M, Eguez RV, Singh H, et al. S-Trap, an Ultrafast Sample-Preparation Approach for Shotgun Proteomics. J Proteome Res. 2018 Sep 7;17(9):2917-2924.
15. Yu F, Haynes SE, Teo GC, et al. Fast Quantitative Analysis of timsTOF PASEF Data with MSFragger and IonQuant. Mol Cell Proteomics. 2020 Sep;19(9):1575-1585.
16. da Veiga Leprevost F, Haynes SE, Avtonomov DM, et al. Philosopher: a versatile toolkit for shotgun proteomics data analysis. Nat Methods. 2020 Sep;17(9):869-870.
17. Kong AT, Leprevost FV, Avtonomov DM, et al. MSFragger: ultrafast and comprehensive peptide identification in mass spectrometry-based proteomics. Nat Methods. 2017 May;14(5):513-520.
18. Verschueren E, Von Dollen J, Cimermancic P, et al. Scoring Large-Scale Affinity Purification Mass Spectrometry Datasets with MiST. Curr Protoc Bioinformatics. 2015 Mar 9;49:8 19 1-8 19 16.
19. Jager S, Cimermancic P, Gulbahce N, et al. Global landscape of HIV-human protein complexes. Nature. 2011 Dec 21;481(7381):365-70.

20. The Gene Ontology C. Expansion of the Gene Ontology knowledgebase and resources. Nucleic Acids Res. 2017 Jan 4;45(D1):D331-D338.
21. Mi H, Muruganujan A, Huang X, et al. Protocol Update for large-scale genome and gene function analysis with the PANTHER classification system (v.14.0). Nat Protoc. 2019 Mar;14(3):703-721.
22. Mi H, Muruganujan A, Ebert D, et al. PANTHER version 14: more genomes, a new PANTHER GO-slim and improvements in enrichment analysis tools. Nucleic Acids Res. 2019 Jan 8;47(D1):D419-D426.
23. Darbellay J, Lai K, Babiuk S, et al. Neonatal pigs are susceptible to experimental Zika virus infection. Emerg Microbes Infect. 2017 Feb 15;6(2):e6.
24. Trus I, Darbellay J, Huang Y, et al. Persistent Zika virus infection in porcine conceptuses is associated with elevated <i>in utero</i> cortisol levels. Virulence2018. p. 21505594.2018.1504558.
25. Xu MY, Liu SQ, Deng CL, et al. Detection of Zika virus by SYBR green one-step real-time RT-PCR. Journal of virological methods: J Virol Methods; 2016. p. 93-97.
26. Eiden M, Vina-Rodriguez A, Hoffmann B, et al. Two new real-time quantitative reverse transcription polymerase chain reaction assays with unique target sites for the specific and sensitive detection of lineages 1 and 2 West Nile virus strains. J Vet Diagn Invest. 2010 Sep;22(5):748-53.
27. Shao N, Li F, Nie K, et al. TaqMan Real-time RT-PCR Assay for Detecting and Differentiating Japanese Encephalitis Virus. Biomedical and environmental sciences : BES: Biomed Environ Sci; 2018. p. 208-214.
28. Chapagain S, Pal Singh P, Le K, et al. Japanese encephalitis virus persists in the human reproductive epithelium and porcine reproductive tissues. PLoS Negl Trop Dis. 2022 Jul;16(7):e0010656.

A
ChIRP-MS
Zika virus
VERO-ZAP-WT
Crosslinking
VERO-ZAP-KO
MOCK
LC-MS/MS
Viral RNA
Proteins
Antisense probe
B
ZAP-WT MOI=10
ZAP-KO MOI=2
C
Log10 ZIKV RNA copies/ml
12
10
8
6
4
2
Input
Enriched
VERO-ZAP-WT
VERO-ZAP-KO
VERO-ZAP-WT
VERO-ZAP-KO
D
Input VERO-ZAP-WT
Input VERO-ZAP-KO
Enriched VERO-ZAP-WT
Enriched VERO-ZAP-KO
Read depth Log10
Zika nucleotide position
0
1
2
3
4
2000
4000
6000
8000
10000

Extended Zika virus RNA interactome
A
DHX15
TRIM56
ACIN1
UPF1
NCOA5
SPATS2L
PURB
PURA
SAFB2
SUGP2
FXR2
YBX1
FMR1
MYEF2
SLTM
0
20
40
60
Spectral counts
D
NUCLEIC ACID BINDING (GO:0003676) (1.14E-39)
mRNA BINDING (GO:0003729) (8.89E-04)
RNA BINDING (GO:0003723) (2.87E-33)
DOUBLE-STRANDED DNA BINDING (GO:0003690) (3.36E-02)
DNA BINDING (GO:0003677) (5.51E-07)
HELICASE ACTIVITY (GO:0004386) (3.15E-02)
SINGLE-STRANDED DNA BINDING (GO:0003697) (3.39E-02)
0
1
2
3
4
5
Fold enrichment
ZAP-independent Zika virus RNA interactome
B
FXR2
ZNF326
TRIM25
CAPG
RBM4B
TRIM56
SUGP2
PURA
SLTM
PBXIP1
PURB
MYEF2
SPATS2L
FMR1
YBX1
0
10
20
Spectral counts
E
RNA BINDING (GO:0003723) (2.65E-02)
0
1
2
3
4
5
Fold enrichment
ZAP-dependent Zika virus RNA interactome
C
STAU2
GTPBP4
DDX42
BOP1
SNW1
RBM12B
SART1
MCM5
DDX27
FAM120C
EFTUD2
DDX23
MCM3
NOP2
RNA helicase
0
10
20
Spectral counts
F
RNA BINDING (GO:0003723) (1.22E-14)
NUCLEIC ACID BINDING (GO:0003676) (2.87E-20)
DNA BINDING (GO:0003677) (3.29E-02)
ACTING ON A NUCLEIC ACID (GO:0140640) (3.15E-02)
SINGLE-STRANDED DNA BINDING (GO:0003697) (4.34E-02)
HELICASE ACTIVITY (GO:0004386) (3.33E-04)
0
1
2
3
4
5
Fold enrichment

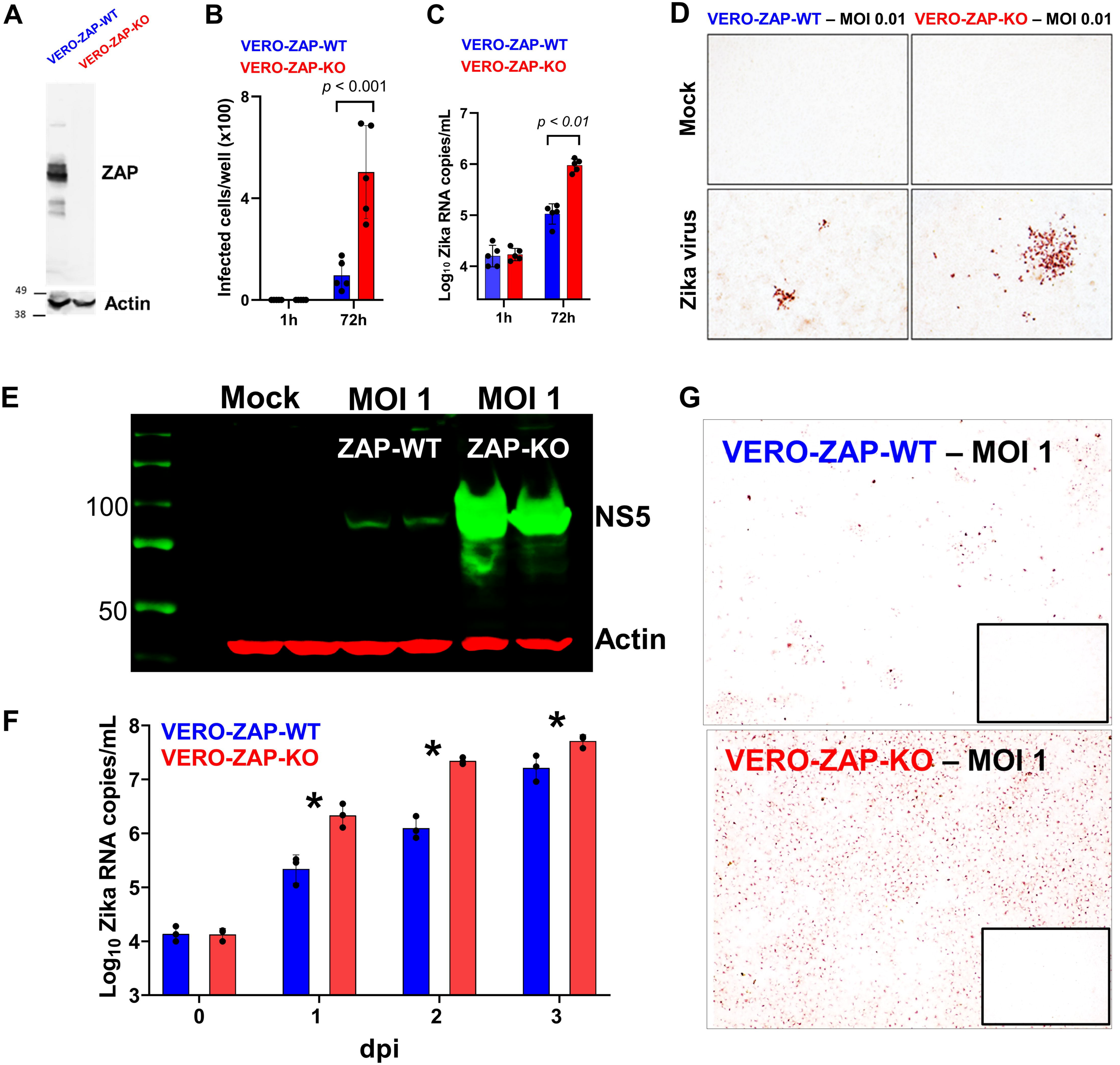
A
VERO-ZAP-WT
VERO-ZAP-KO
ZAP
49
38
Actin
B
VERO-ZAP-WT
VERO-ZAP-KO
$p < 0.001$
Infected cells/well (x100)
8
4
0
1h
72h
C
VERO-ZAP-WT
VERO-ZAP-KO
$p < 0.01$
Log₁₀ Zika RNA copies/mL
7
6
5
4
1h
72h
D
VERO-ZAP-WT – MOI 0.01
VERO-ZAP-KO – MOI 0.01
Mock
Zika virus
E
Mock
MOI 1
MOI 1
ZAP-WT
ZAP-KO
100
50
NS5
Actin
F
VERO-ZAP-WT
VERO-ZAP-KO
Log₁₀ Zika RNA copies/mL
8
7
6
5
4
3
*
*
*
0
1
2
3
dpi
G
VERO-ZAP-WT – MOI 1
VERO-ZAP-KO – MOI 1

JEV
Zika virus
WNV
A
VERO-WT
VERO-ZAP-KO
Mock
JEV
B
JEV E protein positive counts
VERO-ZAP-WT
VERO-ZAP-KO
1500
1200
900
600
300
0
*
Mock
JEV
C
Log10 Fold Change of JEV RNA (1h vs 72h)
6
5
4
3
2
1
0
*
VERO-WT
VERO-ZAP-KO
D
Mock
JEV
ZAP+
ZAP-
100
50
NS5
Actin
E
VERO-WT
VERO-ZAP-KO
Mock
Zika
F
Zika E protein positive counts
VERO-ZAP-WT
VERO-ZAP-KO
2400
2100
1800
1500
1200
900
600
300
0
*
Mock
Zika
G
Log10 Fold Change of Zika RNA (1h vs 72h)
6
5
4
3
2
1
0
*
VERO-WT
VERO-ZAP-KO
H
Mock
Zika
ZAP+
ZAP-
100
50
NS5
Actin
I
VERO-WT
VERO-ZAP-KO
Mock
WNV
J
WNV E protein positive counts
VERO-ZAP-WT
VERO-ZAP-KO
2700
2400
2100
1800
1500
1200
900
600
300
0
*
Mock
WNV
K
Log10 Fold Change of WNV RNA (1h vs 48h)
7
6
5
4
3
2
1
0
VERO-WT
VERO-ZAP-KO
L
Mock
WMV
ZAP+
ZAP-
75
37
NS5
Actin